

Autocrine Fibronectin Inhibits Breast Cancer Metastasis

Aparna Shinde², Sarah Libring³, Aktan Alpsoy², Ammara Abdullah², James A. Schaber⁴, Luis Solorio^{1,3*}, Michael K. Wendt^{1,2*}

Affiliations:

¹Purdue Center for Cancer Research, Purdue University, West Lafayette, Indiana 47907

²Department of Medicinal Chemistry and Molecular Pharmacology, Purdue University, West Lafayette, Indiana 47907

³Department of Biomedical Engineering, Purdue University, West Lafayette, Indiana 47907

⁴Bindley Bioscience Center, Purdue University, West Lafayette, Indiana 47907

Running Title: Autocrine Fibronectin Limits Metastasis

Abbreviations: epithelial-mesenchymal transition (EMT), mesenchymal-epithelial transition (MET), tumor microenvironment (TME), extracellular matrix (ECM), three-dimensional (3D), fibronectin (FN), Molecular Taxonomy of Breast Cancer International Consortium (METABRIC), polystyrene (PS), epithelial cadherin (Ecad), epithelial-mesenchymal heterogeneity (EMH).

*To whom correspondence should be addressed:

Michael K. Wendt, Department of Medicinal Chemistry and Molecular Pharmacology, Purdue University, West Lafayette, IN 47907. Phone: 765-494-0860. Email: mwendt@purdue.edu

Luis Solorio, Department of Biomedical Engineering, Purdue University, West Lafayette, IN 47907. Phone: 765-496-1956. Email: lsolorio@purdue.edu

Disclosure of Potential Conflicts of interest: The authors declare no conflicts of interest.

Abstract

Both epithelial-mesenchymal transition (EMT) and mesenchymal-epithelial transition (MET) are linked to metastasis via their ability to increase invasiveness and enhance tumor-initiating capacity. Growth factors, cytokines and chemotherapies present in the tumor microenvironment (TME) are capable of inducing EMT, but the role of the extracellular matrix (ECM) in this process remains poorly understood. Here, a novel tessellated three-dimensional (3D) polymer scaffolding is used to produce a fibrillar fibronectin matrix that induces a EMT-like event that includes phosphorylation of STAT3 and requires expression of $\beta 1$ integrin. Consistent with these findings, analysis of the METABRIC dataset strongly links high-level fibronectin (FN) expression to decreased patient survival. In contrast, in vitro analysis of the MCF-10A progression series indicated that intracellular FN expression was associated with non-metastatic cells. Therefore, differential bioluminescent imaging was used to track the metastasis of isogenic epithelial and mesenchymal cells within heterogeneous tumors. Interestingly, mesenchymal tumor cells do not produce a FN matrix and cannot complete the metastatic process, even when grown within a tumor containing epithelial cells. However, mesenchymal tumor cells form FN containing cellular fibrils capable of supporting the growth and migration of metastatic-competent tumor cells. Importantly, depletion of FN allows mesenchymal tumor cells to regain epithelial characteristics and initiate in vivo tumor growth within a metastatic microenvironment.

Implications: In contrast to the tumor promoting functions of fibronectin within the ECM, these data suggest that autocrine fibronectin production inhibits the metastatic potential of mesenchymal tumor cells.

Introduction

The ability of epithelial cells to transition into a more primitive, migratory phenotype is an important process that occurs during wound healing and development. However, this capacity of epithelial cells to transition between these different phenotypes also supports the metastatic progression of breast cancer. Numerous model systems suggest that cells undergo a transient epithelial-mesenchymal transition (EMT) during invasion and dissemination, and then reverse that process through mesenchymal-epithelial transition (MET) during the outgrowth of secondary metastatic tumors (1–4). The importance of a highly plastic cell type to overcome the various stresses of the metastatic process is intuitively logical. However, the onset and reversal of EMT have also been linked to the increased tumor initiating capacity (5,6). These studies raise exciting possibilities that EMT:MET may reactivate a fundamental genetic program capable of producing cells with an enhanced potential for adaptation to metastatic microenvironments and initiation of secondary tumors. Concurrent with these single cell autonomous notions of EMT:MET and stemness is a growing concept supporting the importance of EMT-induced tumor cell heterogeneity (7). Heterogeneity within the stromal compartment of tumors is clearly important to metastasis as several critical paracrine signaling axes consisting of growth factors, hormones and adipokines have been described (8–10). However, numerous inducers of EMT can result in subpopulations of tumor cells with unique mechanical and molecular signatures that fall along a spectrum of epithelial to mesenchymal phenotypes (11)(12). Recent evidence suggests that more potent inducers of EMT can push epithelial tumor cells into a highly mesenchymal, stromal-like state and these cells have a reduced ability to undergo MET (13). What the drivers of these more stable mesenchymal phenotypes are, and how and if these stromal-like tumor cells continue to contribute to the metastatic process remains to be established.

In healthy tissues, stromal cells maintain the composition and structure of the tissue through production of extracellular matrix (ECM) proteins and paracrine signaling with epithelial cells (14). Both compositional and structural changes in the ECM have been observed during metastasis (15). One such ECM protein that can be produced by tumor cells following EMT is fibronectin (FN). Overall, increased FN expression in primary mammary tumors is strongly associated with decreased patient survival (16). Herein, we utilize a novel 3D culture system consisting of a tessellated scaffold to demonstrate that fibrillar FN can drive an EMT-like morphological change, that allows for migration and proliferation of metastatic breast cancer cells independent of a hydrogel or polymer support. Counterintuitively, we find that breast cancer cells that constitutively express FN display an extremely stable mesenchymal phenotype and are not capable of completing metastasis. Therefore, we sought to address the hypothesis that autocrine production of FN by tumor cells limits their metastatic potential. Along these lines, genetic depletion of FN, but not its cognate receptor β 1 integrin, allows tumor cells to regain epithelial characteristics and initiate tumor formation in the lungs.

Overall, our studies shed new light on the role of autocrine FN signaling during tumor growth and metastasis. Furthermore, we introduce a robust and versatile 3D cell culture approach capable of accurately recapitulating tumor microenvironment conditions that allow for controlled studies that cannot be accomplished *in vivo* or with other systems.

Materials and Methods

Reagents

Ca1a and Ca1h cells were kindly provided by Dr. Fred Miller (Wayne St. University). These cells were cultured in DMEM containing 10% FBS and pen/strep. Stable expression of the luciferase, eGFP or dTomato was achieved through lenti-viral transduction and selection in puromycin or zeocin. For eGFP and dTomato expression cells were sorted to increase uniform fluorescence across the entire population (Supplementary Fig. 1). Manipulation of FN expression was achieved through lentiviral-mediated transduction of TRCN0000064830, TRCN0000064832, a scrambled control shRNA (GE Dharmacon, Lafayette, CO), or pLV (VectorBuilder, Santa Clara, CA) encoding full length human FN or GFP as a control. In all cases, stable genomic integration of constructs was selected for using puromycin. HMLE cells were kindly provided by Sendurai Mani (MD Anderson Cancer Center). These cells were cultured as previously described (16). Primary human pulmonary fibroblasts were obtained from ATCC and cultured in the recommended fibroblast basal media supplemented with fibroblast growth factor low serum kit (ATCC). Cells were validated for lack of contamination using IDEXX Impact III testing in April 2nd, 2014 and cryogenically frozen. All cell lines were used within one month of thawing.

Animal models

All *in vivo* assays were conducted under IACUC approval from Purdue University. Where indicated control or luciferase expressing Ca1a and Ca1h cells (2×10^6 / 50 μ l) were injected into the second mammary fat pad of female 5-week old, nu/nu mice. Thirty-five days after engraftment tumors were surgically excised and metastasis was subsequently quantified by bioluminescent imaging. In other experiments, control and FN-depleted Ca1h cells (5×10^5 / 100 μ l) were injected into the lateral tail vein of female 4-month-old, NSG mice. Pulmonary tumor

growth was quantified by bioluminescence at the indicated time points. Based on previously established variability for bioluminescent imaging, 5 mice per group was chosen to adequately power our experiments to 0.80, with an α of 0.05.

Immunological assays

For immunoblot analyses cells were lysed using a modified RIPA lysis buffer containing 50 mM Tris, 150mM NaCl, 0.25% Sodium Deoxycholate, 1.0% NP40, 0.1% SDS, protease inhibitor cocktail, 10mM activated sodium ortho-vanadate, 40 mM β -glycerolphosphate and 20mM sodium fluoride. These lysates were separated by reducing SDS PAGE and probed for β 1 integrin, FGFR1 (Cell signaling technologies, Danvers, MA), fibronectin, epithelial cadherin (Ecad), vimentin (BD biosciences, San Jose, CA), zeb1, actin (Santa Cruz Biotechnology, Santa Cruz, CA), zo-1 (Thermofisher Scientific), Ncad (RnD systems) or β -tubulin (DSHB, Iowa City, IA). For immunofluorescence, cells were fixed in 4% paraformaldehyde (PFA), permeabilized in 0.1% triton-X 100 and processed using fluorescently labeled phalloidin (Thermo Fisher, Waltham, MA) for visualization of the actin cytoskeleton, Ecad (BD biosciences) or FN (Abcam, Cambridge, MA). Where indicated, cellular monolayers were removed through incubation with 0.4% triton, 1.5 NaCl, 50 mM, Tris pH 8 and 50mM EDTA for 48h in 4°C, washed with water, incubated with 0.5% sodium deoxycholate at 25°C and finally incubated with PBS (+MgCl₂) for 1 hour. Secreted proteins were precipitated from serum free media by incubating 6 volumes of sample with 1 volume of 50% trichloroacetic acid and 1 volume of 0.1% sodium deoxycholate on ice for 30 minutes. Protein was precipitated via centrifugation and the pellet was twice washed with acetone and finally boiled at 95°C with 500 μ l of 4x laemmlli buffer. For flow cytometry cells were fixed in 1% PFA, blocked in 2.0% bovine serum albumin and stained with CD24 and CD44 (BioLegend, San Diego, CA) that were directly conjugated to the fluorescent

probes. Patient samples stained for FN (DakoCytomation) by immunohistochemistry were obtained from the protein atlas (17,18). Immunohistochemical analyses of formalin fixed paraffin embedded tissue sections from Ca1h pulmonary tumors were conducted by deparafinization in xylene, rehydration, and antigen retrieval using 10mM sodium citrate (pH 6.0) under pressurized boiling. After inactivation of endogenous peroxidases in 3% H₂O₂, primary antibodies specific for Ecad (BD biosciences), human vimentin (BD biosciences), or Ki-67 (BD biosciences), or FN (BD biosciences) were added to serial sections and incubated overnight. Protein specific staining was detected through the use of appropriate biotinylated secondary antibodies in conjunction with ABC reagent (Vector, Burlingame, CA). These sections were counterstained with hematoxylin, dehydrated, and mounted.

3D hydrogel assays

Fluorescent and bioluminescent Ca1a cells were mixed with non-labeled or fluorescent Ca1a, Ca1h control, and Ca1h cells depleted in FN in 1:1 ratios and grown under 3D culture conditions. Cell growth was quantified via addition of luciferin (GoldBio, St. Louis, MO). Briefly, 2000 cells were plated in each well of a white-walled 96-well dish on top of a solidified 50μl bed of Cultrex basement membrane extract (BME) from (Trevigen, Gaithersburg, MD). These cells were suspended in growth media containing DMEM, 10% FBS and 5% of the BME. For confocal microscopy, differentially labelled cells were grown under 3D culture conditions using 50 mm Dish (MatTek, Ashland, MA) and images were taken at using Zeiss 40x water dipping objective lens.

Production of 3D scaffolds

Scaffolds were produced using a photolithography based approach, using the negative photo resist SU-8 2050 (Microchem, Westborough, MA). Silicon wafers were cleaned using a Glen

1000P plasma cleaner, and dehydrated by baking at 120°C for 5 min. Omnicoat (Microchem, Westborough, MA) was used as a sacrificial layer. 3 layers of Omnicoat were applied for each wafer using a spin coater at a spread speed of 500 RPM for 5 s, followed by 30 s at 1000 RPM. After each layer was applied, the wafer was baked at 200°C for 1 min, then allowed to cool to RT. The SU-8 was then coated onto the wafer using a spread speed of 500 RPM for 5 s, followed by 1700 RPM for 30 s. A final thickness of approximately 100 µm was attained. The wafer was then allowed to degass overnight at RT. After degassing, the wafers were baked at 65°C for 10 min, then the temperature was increased to 95°C for an additional 50 min bake. The wafers were then exposed to UV light using an MJB 45S mask aligner in hard contact mode, with a 20 second exposure time. A photomask was used to create the desired geometric pattern. After exposure, the wafer was baked for 5 min at 65°C followed by 10 min at 95°C. After cooling to RT, the wafers were developed in SU-8 developer for 11 min, rinsed in isopropanol (IPA), and then dried using compressed nitrogen gas. The developed scaffolds were then hard baked for 15 min at 150°C, and then released from the wafer using fresh SU-8 developer. The scaffolds were subsequently washed 6 times in IPA and allowed to dry overnight before use.

Fibronectin coating of scaffolds

Scaffolds were coated with fibronectin by first mounting the scaffolds to a ferrous magnetic stainless steel frame using a cyanoacrylate based adhesive. The mounted scaffolds were then placed in a 100 µg/mL solution of fibronectin, and then magnetically suspended at the air-water interface. The scaffolds were rotated for 2 h on a rotisserie shaker that was maintained at 30°C with a rate of rotation of 8 RPM.

3D scaffold assays

Uncoated or fibronectin coated 3D scaffolds were placed in ultralow attachment 24-well dishes. Cells (50,000) were added to the scaffolds for 24 hours at which point non-adherent cells were washed away. For immunofluorescence, at day 6 the scaffolds containing the cells were fixed and stained with the indicated antibodies using protocols described above. Images were taken using Zeiss 40x water dipping objective lens.

mRNA analyses

RNA was isolated using RNA isolation kit (Omega bio-tek, Norcross, GA). Total RNA was reverse-transcribed using a cDNA synthesis kit from (Thermo Fisher) and semi quantitative real-time PCR was performed using iQ SYBR Green (Thermo Fisher). The following primers were used for the analysis. *FN1* sense; ACAAACACTAATGTTAATTGCCCA, *FN1* antisense; CCTCCAGAGCAAAGGGCTTA, *CDH1* sense; GTTCAGACTCCAGCCCCGC, *CDH1* antisense; AAATTCACTCTGCCAGGACG, *VIM* sense; CGGGAGAAATTGCAGGAGGA, *VIM* antisense; AAGGTCAAGACGTGCCAGAG

Statistical analyses

2-way ANOVA or 2-sided T-tests were used where the data met the assumptions of these tests and the variance was similar between the two groups being compared. P values of less than 0.05 were considered significant. No exclusion criteria were utilized in these studies.

Results

Fibronectin expression is associated with decreased patient survival

We have previously demonstrated an association between FN expression and decreased patient survival (16). Here we analyzed the recent Molecular Taxonomy of Breast Cancer International Consortium (METABRIC) dataset consisting of more than 2,000 patient tumor biopsies (19).

Significant outliers were observed in every subtype, with the claudin-low subtype having the outliers with the highest overall expression (Fig. 1A). When the dataset is taken as a whole, those patients above the mean or median expression level of FN demonstrated decreased survival compared to those patients below the mean or median (Fig. 1B and not shown). Finally, when separated into quartiles those patients with the highest levels of FN demonstrate the shortest survival time (Fig. 1C). Overall, these data clearly indicate that high-level expression of the FN in primary tumors is strongly associated with decreased patient survival.

Non-metastatic mesenchymal tumor cells aid the metastasis of responder cells within heterogeneous tumors

The MCF10CA1a (Ca1a) and the MCF10CA1h (Ca1h) cells are variants derived from the RAS-transformed MCF-10AT cells (20,21). In culture, whole cell lysates obtained from Ca1h cells demonstrate constitutive expression of FN and low levels of the epithelial marker, Ecad (Fig. 2A). In contrast, Ca1a cells fail to express detectable levels of FN but express robust amounts of Ecad (Fig. 2A). Somewhat counter to the patient data presented in Figure 1, the FN-expressing Ca1h cells are considered to be invasive but not metastatic, while the Ca1a cells are considered to be fully metastatic (21). However, it is difficult to directly compare the differential metastatic potential of the Ca1h and Ca1a cells *in vivo* due to drastic differences in primary tumor growth rates (Ca1h = 65.0 mg ± 17.32 mg; Ca1a = 983.4 mg ± 264 mg, 35 days post mammary fat pad engraftment of 2x10⁶ cells). Furthermore, the metastatic rate of Ca1a primary tumors is very low, making inhibition of this process statistically challenging (Fig. 2B and 2C). Therefore, we sought to create mosaic tumors containing both Ca1h and Ca1a cells and track the metastasis of each cell type independently through differential labeling with firefly luciferase. Using this approach,

1:1 mixtures of Ca1a and Ca1h cells were orthotopically engrafted onto the mammary fat pad of nu/nu mice and these mosaic tumors were grown for 35 days (Fig. 2B). The primary tumors were surgically resected and the subsequent metastasis of each cell type was tracked by firefly bioluminescence (Fig. 2B and 2C). This approach indicated that even in a heterogeneous primary tumor, the Ca1a cells are clearly the cell type that forms metastatic lesions (Fig. 2B and 2C and Supplementary Fig. 2). These studies also revealed a highly significant increase in the metastatic efficiency of the Ca1a cells when grown in a mosaic tumor with the highly mesenchymal Ca1h cells (Fig. 2B and 2C). These data clearly indicate that while not competent for metastasis themselves, constitutively mesenchymal tumor cells can facilitate the metastasis of responder tumor cells in a paracrine manner.

Functionalized FN fibrils facilitate transient EMT and directional cellular migration

Previous studies suggest that FN contributes to metastasis through the induction of EMT (22,23). To further characterize the role of FN in facilitating the heterotypic interactions between Ca1a and Ca1h cells we initially attempted to use the Ca1h cells to create extracellular protein matrixes. However, consistent with previous studies we observed that unlike fibroblasts, Ca1h cells do not deposit FN into a matrix (Fig. 3A and 3B)(24). Therefore, we used a static adsorption coating method to coat tissue culture polystyrene (PS) with exogenous FN. Using this approach, we did observe increased cellular adhesion that was dependent on $\beta 1$ integrin, a critical component of the FN receptor (Supplementary Fig. 3A-3B). Consistent with previous reports, culturing the Ca1a cells on FN coated PS did result in detectable modulation of EMT markers at the mRNA level (Supplementary Fig. 3C). However, using this approach we did not observe a morphological change in the Ca1a cells and we did not observe detectable changes in Ecad

protein levels in these cells even after six consecutive passages on FN coated plates (Supplementary Fig. 3D-3E).

To achieve the fibrillar confirmation of FN that largely exists *in vivo*, we engineered a tessellated scaffold with $500 \mu\text{m}^2$ square pores, made of SU-8, which are capable of supporting the growth of cells when placed in nonadherent culture wells (Fig. 4A; Supplementary Fig. 4) (25,26). In contrast to static adsorption to a growth surface we were able to create fibrillar FN by utilizing a rotational method to coat our 3D cell culture scaffolds (Fig. 4B). Importantly, only these FN fibrils contained cryptic binding domains, indicating enhanced functionalization of the ECM protein (Fig. 4B). The FN fibrils crossed the open spaces of the tessellated scaffold creating a controlled microenvironment for culture of the Ca1a cells free of interference from the polymer scaffold (Fig. 5A). Consistent with our coating of 2D polystyrene, Ca1a cells that remained on the solid support of the FN-coated scaffold maintained cell-cell junctions (Fig. 5A). However, the Ca1a cells that grew off the scaffold within the unsupported FN fibrils underwent an EMT-like morphological change, characterized by activation of the cytoskeleton, dissolution of adherens junctions and detection of STAT3 phosphorylation (Fig. 5A-5C and Supplementary Fig. 5). These effects of fibrillar FN required expression of $\beta 1$ integrin in the Ca1a cells (Fig. 5A-5C and Supplementary Fig. 5). We were able to use time lapse microscopy to capture Ca1a cells migrating and proliferating on these pure FN fibrils (Supplementary video 1).

To quantify this small subpopulation of cells growing within the FN fibrils, off the support of the scaffold, we assessed changes in the CD44 and CD24 populations by flow cytometry. A small but distinct population of Ca1a cells isolated from the FN coated scaffolds demonstrated a mesenchymal $\text{CD44}^{\text{hi}}/\text{CD24}^{\text{lo}}$ phenotype as compared to those same cells harvested from 2D polystyrene (Fig. 5D). This affect was again dependent on the expression of the FN receptor, $\beta 1$

integrin (Fig. 5D). Similar to the Ca1a cells, culture of immortalized human mammary epithelial (HMLE) cells on functionalized FN-coated scaffolds also resulted in the emergence of a CD44^{hi}, mesenchymal population that could be readily visualized upon return to 2D culture (Supplementary Fig. 6) (5,27).

Autocrine expression of fibronectin stabilizes a constitutive mesenchymal phenotype

In contrast, to the requirement of $\beta 1$ integrin for cellular response to fibrillar FN, depletion of $\beta 1$ integrin or pharmacological inhibition of integrin:FAK signaling using cyclic peptides or small molecules kinase inhibitors in the Ca1h cells did not result in a return of epithelial characteristics (Supplementary Fig. 7A-8B). In fact, shRNA-mediated depletion of $\beta 1$ integrin led to increased levels of intracellular FN and diminution in Ecad expression in the T1K cells, an isogenic counterpart of the Ca1h cells (Supplementary Fig. 7A). Therefore, we sought to investigate potential integrin-independent functions of FN in EMT and metastasis that may be working in an intracellular fashion. Confocal microscopy confirmed strong colocalization of intracellular FN with the actin cytoskeleton (Supplementary Fig. 8). Depletion of FN in the Ca1h cells using two independent shRNAs led to increased transcript levels of the epithelial marker Ecad and loss of the mesenchymal marker vimentin, the intensity of which was consistent with the efficiency of FN depletion (Fig. 6A). Additionally, depletion of FN caused altered protein expression of several but not all makers of MET including Ecad, Vimentin, Zeb1, Zo1, FGFR1 and cell surface expression of CD44 and CD24 (Fig. 6B and 6C). Accompanying these phenotypic markers, depletion of FN also lead a robust morphological change in the Ca1h cells, resulting in the reduction of filamentous actin and the formation of adherens junctions (Figs. 6D and 6E). Taken

together, these data are consistent with the conclusion that autocrine FN functions in a $\beta 1$ integrin independent fashion to maintain a stable mesenchymal phenotype.

Tumor cells expressing FN act in a stromal capacity to support the growth of other tumor cells

We next sought to characterize the interaction between FN-producing, constitutively mesenchymal tumor cells and metastatic tumor cells. To this end, we differentially identified Ca1a and Ca1h cells via stable expression and fluorescence activated cell sorting for d-Tomato and eGFP, respectively (Supplementary Fig. 1). These cells were then cultured in a 3D hydrogel basement membrane matrix to assess the growth of the Ca1a cells alone or when in a heterogeneous coculture with the Ca1h cells. Growth of the Ca1a cells alone results in cell dense, spherical 3D structures (Fig. 7A). However, coculture of the Ca1a cells with FN-expressing Ca1h cells resulted in a loss of the spherical morphology, heterogeneous cell interspersion, and enhanced invasion of the Ca1a cells into the surrounding matrix (Fig. 7B, top panels). Additionally, even when cells grew in close physical proximity, they did not form interspersed structures and the spherical growth pattern of the Ca1a structures was maintained (Fig. 7B, middle and bottom panels). Measuring bioluminescence production from the firefly luciferase expressing Ca1a cells allowed us to quantify their increased growth when in the presence of Ca1h cells (Fig. 7C). Decreased formation of heterogeneous cell clusters prevented this stromal support upon FN depletion in the Ca1h cells (Fig. 7C and 7D). These data suggest that FN expression by tumor cells allows them to act in a stromal fashion to physically support the growth of metastatic tumor cells.

Autocrine FN inhibits pulmonary tumor outgrowth

To more specifically characterize the autocrine versus paracrine role of FN in tumor growth we cultured control and FN-depleted Ca1h cells on our 3D scaffolds lacking any exogenous matrix coating. Addition of the Ca1h cells to the 3D scaffolds led to the formation of cellular fibrils that crossed the open spaces of the culture scaffolds (Fig. 8A; Supplementary video 2). In contrast, Ca1h cells depleted in FN expression grew more robustly than control cells (Fig. 8B). However, FN-depleted cells remained on the solid support of the scaffold in an epithelial fashion, generating very distinct cortical actin (Fig. 8A-8C; Supplementary video 3-4). Using our differentially labeled Ca1a and Ca1h cells, we were able to capture time lapse microscopy demonstrating the ability of the Ca1a cells to utilize Ca1h cellular fibrils to migrate away from the culture scaffold (Supplementary video 5-7). These data clearly demonstrate the ability of mesenchymal tumor cells to produce FN-containing cellular fibrils that are capable of facilitating cellular migration of metastatic tumor cells.

The increased proliferation of FN-depleted cells suggested that autocrine FN actively inhibits the ability of tumor cells to grow in a 3D environment. Along these lines, FN is also constitutively expressed by the D2.OR cell model of systemic dormancy as compared to their isogenic and fully metastatic, D2.A1, counterparts (Supplementary Fig. 9)(24). Therefore, we conducted tail vein injection experiments to assess the *in vivo* capacity of control and FN-depleted Ca1h cells to initiate tumor growth within a physiologically relevant site of metastasis. Injection of control Ca1h cells resulted in detectable, but asymptomatic maintenance of these cells in the lungs over a period of 7 weeks (Fig. 8D-8F). In contrast, FN-depleted Ca1h cells were capable of forming numerous macroscopic tumors within the pulmonary microenvironment (Fig. 8D-8F). The bioluminescent signal from mice bearing control Ca1h cells was histologically located to a few small lesions within the lung (Fig. 8F, Supplementary Fig. 10). Consistent with

our *in vitro* data, these smaller lesions that did form contained intracellular FN, but also demonstrated readily detectable levels of Ecad (Fig. 8F). Finally, we were unable to achieve stable overexpress FN in the Ca1a cells to a level that was consistent with that of the Ca1h cells (Fig. 8G). Nonetheless, even this moderate level of autocrine FN expression in the Ca1a cells was sufficient to modulate EMT markers, induce cellular fibril formation, decrease cell growth and inhibit pulmonary tumor formation upon tail injection (Fig. 8G-HIJ). Taken together, these data suggest that when presented as a homogenous inoculum, highly mesenchymal cells can undergo MET in the pulmonary microenvironment and proceed to macroscopic pulmonary tumor formation. However, these events are clearly inhibited by autocrine expression of FN.

Discussion

Patient data presented here and elsewhere clearly demonstrate that high-level expression of FN within primary breast tumors is associated with decreased patient survival (28)(16). These clinical data are somewhat counter to data from tumor cell lines in which constitutive expression of autocrine FN corresponds to a non-metastatic phenotype. Our cell labeling data clearly demonstrate that FN produced by tumor cells that have undergone an EMT contributes to the invasion and metastasis of their epithelial counterparts. Furthermore, our genetic depletion and overexpression studies indicate that production of FN stabilizes a non-metastatic mesenchymal phenotype in an integrin independent manner. The current study supports the concept of epithelial-mesenchymal heterogeneity (EMH). In this scenario, stably mesenchymal tumor cells lose their cell autonomous capacity for metastasis, but still contribute to metastatic progression by taking on a stromal role within the tumor microenvironment.

Consistent with our previous studies, we demonstrate that $\beta 1$ integrin is required for fibrillar FN to promote the phosphorylation of STAT3, a molecule that is known to participate in the induction of EMT (16,29). However, our data also suggest that cellular binding to fibrillar FN physically distorts cell morphology promoting a more mechanically induced mesenchymal morphology. Further understanding of how fibrillar FN alters cell morphology and how these events relate to more transcriptionally driven EMT events induced by drugs and cytokines are clearly warranted. Additionally, our studies suggest the concept of intracrine FN signaling. Indeed, as opposed to its requirement for response to fibrillar FN, depletion of $\beta 1$ integrin does not cause an epithelial reversion as we observe upon depletion of FN. In fact, depletion of $\beta 1$ integrin increased the levels of intracellular FN and enhanced a mesenchymal phenotype. While depletion of $\beta 1$ integrin can have pleiotropic effects on cells, these data are consistent with a

mechanism by which integrins facilitate the secretion of FN, a process that remains poorly understood in epithelial-derived cells. Additionally, our microscopy studies suggest that intracellular FN directly interacts with the actin cytoskeleton, but more nanoscale analyses of these interactions are required. This and other potential mechanisms of how intracrine FN signaling may influence cell morphology and the molecular mechanisms that sustain constitutive FN expression in epithelial-derived tumor cells are areas of current investigation in our lab.

In addition to furthering our biological understanding of FN function and ECM-induced morphological changes, a major advance of the current study is development and implementation of our tessellated cell culture device capable of accurately recapitulating cellular and matrix phenotypes observed *in vivo*. Overall, our culture system represents advanced engineering that is easy to use and inexpensive to produce. As shown, cells cultured on ECM-coated or uncoated scaffolds can be readily grown and analyzed by immunofluorescence, harvested for immunoblot or mRNA analyses, trypsinized for flow cytometry, or passaged for continuous culture. All of these procedures can be done using techniques that are completely analogous to those currently used for standard 2D cell culture. Therefore, while other 3D culture systems are cumbersome and/or cost prohibitive for ongoing culture of stock cells our platform is well suited for long-term maintenance of cultured cell lines or primary, patient-derived tumor tissues.

In conclusion, we observed single-cell migration, loss of junctional Ecad, phosphorylation of STAT3 and gain of CD44 in cells cultured on FN fibrils. However, our studies do not rule out the possibility of tumor cells remaining in a transcriptionally epithelial state while migrating on cellular or FN fibrils. What is clear is that growth, migration and overall metastasis of epithelial-mesenchymal malleable tumor cells is enhanced when in the presence of constitutively mesenchymal, FN-expressing tumor cells. These combined concepts of epithelial-mesenchymal

plasticity and heterogeneity are likely both at play during metastasis, and model-dependent reliance on one or the other likely explains discrepancies between studies as to whether or not EMT contributes to metastasis (27)(28)(30,31).

Acknowledgments

This research was supported in part by the American Cancer Society (RSG-CSM130259) to M. Wendt and the National Institutes of Health (R01CA207751) to M. Wendt and (R00CA198929) to L. Solorio, and the Purdue Center for Cancer Research via an NCI center grant (P30CA023168). We kindly acknowledge the expertise of the personnel within the Purdue Center for Cancer Research Biological Evaluation Core. We also acknowledge the use of the facilities within the Bindley Bioscience Center, a core facility of the NIH-funded Indiana Clinical and Translational Sciences Institute.

References

1. Mani SA, Guo W, Liao M-J, Eaton EN, Ayyanan A, Zhou AY, et al. The epithelial-mesenchymal transition generates cells with properties of stem cells. *Cell*. 2008;133:704–15.
2. Yang J, Mani SA, Donaher JL, Ramaswamy S, Itzykson RA, Come C, et al. Twist, a master regulator of morphogenesis, plays an essential role in tumor metastasis. *Cell*. 2004;117:927–39.
3. Wendt MK, Taylor MA, Schiemann BJ, Schiemann WP. Down-regulation of epithelial cadherin is required to initiate metastatic outgrowth of breast cancer. *Mol Biol Cell*. 2011;22:2423–35.
4. Wendt MK, Taylor MA, Schiemann BJ, Sossey-Alaoui K, Schiemann WP. Fibroblast growth factor receptor splice variants are stable markers of oncogenic transforming growth factor β 1 signaling in metastatic breast cancers. *Breast Cancer Res BCR*. 2014;16:R24.
5. Schmidt JM, Panzilius E, Bartsch HS, Irmler M, Beckers J, Kari V, et al. Stem-Cell-like Properties and Epithelial Plasticity Arise as Stable Traits after Transient Twist1 Activation. *Cell Rep*. 2015;10:131–9.
6. Li R, Liang J, Ni S, Zhou T, Qing X, Li H, et al. A mesenchymal-to-epithelial transition initiates and is required for the nuclear reprogramming of mouse fibroblasts. *Cell Stem Cell*. 2010;7:51–63.
7. Neelakantan D, Zhou H, Oliphant MUJ, Zhang X, Simon LM, Henke DM, et al. EMT cells increase breast cancer metastasis via paracrine GLI activation in neighbouring tumour cells. *Nat Commun*. 2017;8:ncomms15773.
8. Wyckoff J, Wang W, Lin EY, Wang Y, Pixley F, Stanley ER, et al. A paracrine loop between tumor cells and macrophages is required for tumor cell migration in mammary tumors. *Cancer Res*. 2004;64:7022–9.
9. Fillmore CM, Gupta PB, Rudnick JA, Caballero S, Keller PJ, Lander ES, et al. Estrogen expands breast cancer stem-like cells through paracrine FGF/Tbx3 signaling. *Proc Natl Acad Sci*. 2010;107:21737–42.
10. Dieudonne M-N, Machinal-Quelin F, Serazin-Leroy V, Leneveu M-C, Pecquery R, Giudicelli Y. Leptin mediates a proliferative response in human MCF7 breast cancer cells. *Biochem Biophys Res Commun*. 2002;293:622–8.
11. Pastushenko I, Brisebarre A, Sifrim A, Fioramonti M, Revenco T, Boumahdi S, et al. Identification of the tumour transition states occurring during EMT. *Nature*. 2018;1.
12. Jolly MK, Ware KE, Gilja S, Somarelli JA, Levine H. EMT and MET: necessary or permissive for metastasis? *Mol Oncol*. :n/a-n/a.

13. Kuo AH, Qian D, Scheeren FA, Dirbas FM, Somlo G, Zabala M, et al. Role of epithelial to mesenchymal transition associated genes in mammary gland regeneration and breast tumorigenesis. *Nat Commun*. 2017;8:1669.
14. Bani D, Nistri S. New insights into the morphogenic role of stromal cells and their relevance for regenerative medicine. lessons from the heart. *J Cell Mol Med*. 2014;18:363–70.
15. Provenzano PP, Eliceiri KW, Campbell JM, Inman DR, White JG, Keely PJ. Collagen reorganization at the tumor-stromal interface facilitates local invasion. *BMC Med*. 2006;4:38.
16. Balanis N, Wendt MK, Schiemann BJ, Wang Z, Schiemann WP, Carlin CR. Epithelial to mesenchymal transition promotes breast cancer progression via a fibronectin-dependent STAT3 signaling pathway. *J Biol Chem*. 2013;288:17954–67.
17. Berglund L, Björling E, Oksvold P, Fagerberg L, Asplund A, Szigyarto CA-K, et al. A gene-centric Human Protein Atlas for expression profiles based on antibodies. *Mol Cell Proteomics MCP*. 2008;7:2019–27.
18. Uhlén M, Björling E, Agaton C, Szigyarto CA-K, Amini B, Andersen E, et al. A human protein atlas for normal and cancer tissues based on antibody proteomics. *Mol Cell Proteomics MCP*. 2005;4:1920–32.
19. Curtis C, Shah SP, Chin S-F, Turashvili G, Rueda OM, Dunning MJ, et al. The genomic and transcriptomic architecture of 2,000 breast tumours reveals novel subgroups. *Nature*. 2012;486:346–52.
20. Strickland LB, Dawson PJ, Santner SJ, Miller FR. Progression of premalignant MCF10AT generates heterogeneous malignant variants with characteristic histologic types and immunohistochemical markers. *Breast Cancer Res Treat*. 2000;64:235–40.
21. Santner SJ, Dawson PJ, Tait L, Soule HD, Eliason J, Mohamed AN, et al. Malignant MCF10CA1 cell lines derived from premalignant human breast epithelial MCF10AT cells. *Breast Cancer Res Treat*. 2001;65:101–10.
22. Li C-L, Yang D, Cao X, Wang F, Hong D-Y, Wang J, et al. Fibronectin induces epithelial-mesenchymal transition in human breast cancer MCF-7 cells via activation of calpain. *Oncol Lett*. 2017;13:3889–95.
23. Park J, Schwarzbauer JE. Mammary epithelial cell interactions with fibronectin stimulate epithelial-mesenchymal transition. *Oncogene*. 2014;33:1649–57.
24. Ruoslahti E. Fibronectin in cell adhesion and invasion. *Cancer Metastasis Rev*. 1984;3:43–51.
25. To WS, Midwood KS. Plasma and cellular fibronectin: distinct and independent functions during tissue repair. *Fibrogenesis Tissue Repair*. 2011;4:21.

26. Moon P-G, Lee J-E, Cho Y-E, Lee SJ, Chae YS, Jung JH, et al. Fibronectin on circulating extracellular vesicles as a liquid biopsy to detect breast cancer. *Oncotarget*. 2016;7:40189–99.
27. Brown W, Akhand S, Wendt M. FGFR signaling maintains a drug persistant cell population following epitheial-mesenchymal transistion. *Oncotarget*. 2016;
28. Fernandez-Garcia B, Eiró N, Marín L, González-Reyes S, González LO, Lamelas ML, et al. Expression and prognostic significance of fibronectin and matrix metalloproteases in breast cancer metastasis. *Histopathology*. 2014;64:512–22.
29. Wendt MK, Balanis N, Carlin CR, Schiemann WP. STAT3 and epithelial-mesenchymal transitions in carcinomas. *JAK-STAT*. 2014;3:e28975.
30. Fischer KR, Durrans A, Lee S, Sheng J, Li F, Wong STC, et al. Epithelial-to-mesenchymal transition is not required for lung metastasis but contributes to chemoresistance. *Nature* [Internet]. 2015 [cited 2015 Nov 13];advance online publication. Available from: <http://www.nature.com/nature/journal/vaop/ncurrent/full/nature15748.html#>
31. Zheng X, Carstens JL, Kim J, Scheible M, Kaye J, Sugimoto H, et al. Epithelial-to-mesenchymal transition is dispensable for metastasis but induces chemoresistance in pancreatic cancer. *Nature*. 2015;527:525–30.

Figure Legends

Figure 1. FN expression is associated with decreased patient survival. (A) The METABRIC dataset was divided into breast cancer subtypes as determined by the PAM50 and analyzed for expression of *FN1*. Differences in FN1 expression between subtypes were analyzed by ANOVA resulting in the indicated *P* values. (B) Patients were separated into two groups based on the mean expression value of *FN1* and overall survival was plotted. (C) Patients were separated into quartiles based on FN1 expression and overall survival was plotted. Data in panels B and C were analyzed by a Log-rank test resulting in the indicated *P* values.

Figure 2. FN expressing tumor cells support the metastasis of epithelial cells from heterogeneous primary tumors. (A) Immunoblot analyses for fibronectin (FN) and epithelial cadherin (Ecad) from nonmetastatic Ca1h cells and metastatic Ca1a cells. (B) Ca1a and Ca1h cells differentially expressing firefly luciferase were engrafted onto the mammary fat pad of two separate groups of mice. Bioluminescent images were taken immediately after engraftment (Day 0) and 95 days later (Day 95). (C) Primary mammary tumors were removed 35 days after engraftment and whole mouse bioluminescence at day 95 was used to quantify metastatic recurrence. Data are presented as the natural log (LN) of the bioluminescent radiance for each mouse ($n=5$ mice per group), resulting in the indicated *P* value.

Figure 3. Tumor cells do not deposit fibronectin into a fibrillar matrix. (A) Human pulmonary fibroblasts (HPF) and Ca1h cells were gathered via trypsinization, washed to remove extracellular proteins and subsequently lysed to obtain whole cell lysates (WCL). Separate, confluent cultures of HPFs or Ca1h cells were decellularized and deposited matrix proteins were gathered with SDS containing lysis buffer. Finally, serum free media from confluent monolayers of HPFs and Ca1h cells was concentrated by protein precipitation. These three separate fractions were analyzed by immunoblot for the presence of FN. Expression of β -tubulin (β -tub) served as a loading control for the WCL. (B) Confluent cultures of Ca1h and HPFs were decellularized as in panel A and the remaining matrix was stained with antibodies specific for fibronectin.

Figure 4. Fabrication and matrix coating of tessellated culture scaffolds. (A) A sacrificial layer of omnicoat (red) is added to a silicon wafer (gray). Next, the negative resist SU-8 is coated

onto the wafer (black), followed by a soft bake. After the soft bake the wafers are exposed to UV light, followed by development of the wafer. After development, regions in the SU-8 layer that were not exposed to UV light are removed, leaving behind the scaffolds on the silicon wafer. The sacrificial layer is then removed, allowing for release of the scaffolds from the silicon, which can then be used for cell culture applications. (B) These scaffolds were coated with fibronectin using both static surface adsorption as well as rotational coating. Static adsorption of the scaffolds with fibronectin resulted in a conformal layer of the protein, that was absent of fibrils. After rotational coating fibronectin fibrils formed, that spanned the free volume of the scaffolding. Immunostaining revealed that surface adsorption of the scaffolds did not expose the cryptic binding domain of functionalized FN (Fn-3). However, after rotational coating this domain is exposed.

Figure 5. Functionalized fibronectin fibrils facilitate EMT and directional cellular migration. (A) Control (scram) and β 1 integrin depleted (sh β 1 Int) Ca1a cells were cultured on fibronectin coated 3D scaffolds as described in the methods for 6 days and images were acquired using phase contrast microscopy. Arrows indicate single cells (scram) or cell clusters (sh β 1 Int) growing off of the solid support of the scaffold. (B and C) The cells cultured as described in panel A were stained with antibodies against Ecad in panel B or phospho-STAT3 in panel C. In both cases cells were counter stained with phalloidin (red) and dapi (blue) to visualize the actin cytoskeleton and the nucleus, respectively. (D) Control (scram) and β 1 integrin depleted (sh β 1 Int) Ca1a cells were cultured on fibronectin coated 3D scaffolds or polystyrene (PS) for 6 days and analyzed by flow cytometry for cell surface expression of CD44 and CD24.

Figure 6. Expression of fibronectin stabilizes a mesenchymal phenotype. (A) Control (scram) or two independent shRNAs, shFN30 or shFN32, targeting human *FN1* transcripts were stably expressed in the Ca1h cells. Transcript levels for fibronectin (*FN1*), E-cadherin (*CDH1*) and vimentin (*VIM*) were quantified relative to control Ca1h cells. (B) Immunoblot analyses for FN, Ecad and Vimentin (Vim), Zeb1, Zo1, FGFR1, β 1 integrin, N-cadherin (Ncad), from control (scram) and FN-depleted Ca1h cells. Levels of these proteins in the Ca1a cells is shown as a reference. Expression of β -tubulin served as a loading control. (C) Control and FN-depleted Ca1h cells were analyzed by flow cytometry for cell surface expression of CD44 and CD24. (D) Phase contrast images showing the differential morphologies of control and FN-depleted Ca1h

cells. (E) Control (scram), and FN-depleted (shFN30 and shFN32) Ca1h cells were immunostained for Ecad (green), and stained with phalloidin (red) and dapi (blue) to visualize the actin cytoskeleton and nuclei, respectively. Confocal images shown are z, x and y planes reconstructed from serial sections obtained throughout whole cells. All data are representative of at least three independent experiments.

Figure 7. Depletion of FN decreases the stromal support capacity of breast cancer cells. Confocal images of dTomato expressing Ca1a cells cultured for 16 days under 3D hydrogel conditions, alone (A) and with eGFP labelled Ca1h scram (B, top), shFN30 (B, middle), shFN32 (B, bottom) cells. (B) *Left panels*: Confocal images are z, x and y planes reconstructed from serial sections obtained throughout the entire cell cluster. *Right panels*: Three-dimensional projections of cell clusters imaged with confocal sectioning. (C) Bioluminescent Ca1a cells were cocultured with or without non-bioluminescent Ca1a, control Ca1h (scram), or FN depleted Ca1h (shFN30 or shFN32) cells under 3D hydrogel conditions in a 1:1 ratio. Data are day 16 Ca1a-derived luminescence values relative to the day 0 luminescence values. Data are the mean values (\pm SE) of at least three independent experiments completed in triplicate, resulting in the indicated P values. (D) Fluorescently labeled Ca1a and Ca1h cells were mixed at 1:1 ratios, cultured in a 3D hydrogel for 4 days and the numbers of heterogeneous cell clusters containing both d-Tomato and eGFP positive cells were quantified. Data are the mean (\pm SE) number of heterogeneous cell clusters per field of view over 9 separate fields resulting in the indicated P value.

Figure 8. Autocrine FN inhibits pulmonary tumor formation. (A) Control (scram) and FN depleted (shFN30 and shFN32) Ca1h cells were cultured on 3D scaffolds as described in the methods for 6 days and images were acquired using phase contrast microscopy. (B) Growth of control (scram) and FN-depleted (shFN30) Ca1h cells was quantified by cell titer glow assay at the indicated time points. Data are the mean arbitrary luminescence units (ALU) (\pm SE) for three independent experiments completed in triplicate resulting in the indicated P value. (C) Control (scram) and FN depleted (shFN30) Ca1h cells were cultured on the 3D scaffold system for 6 days and subsequently stained with antibodies against FN (green), phalloidin (red) and dapi (blue). z, x and y planes are shown from reconstructed serial sections obtained through whole cells. *Right panels*: three-dimensional projections of cells shown in the left panels. (D)

Bioluminescent images of representative mice taken immediately (Day 0) and 35 days (Day 35) following tail vein injection of control (scram) and FN-depleted (shFN30) Ca1h cells. (E) The mean (\pm SE) pulmonary bioluminescence values normalized to the injected values (n=3 mice for scram, n=5 mice for shFN30) were quantified at the indicated time points, resulting in the indicated P value. (F) Resultant pulmonary tumors from control (scram) and FN-depleted (shFN30) Ca1h cells were analyzed by histology. Serial sections were stained with hematoxylin and eosin (H&E) or analyzed by immune staining for Vimentin, FN, and Ecad. (G) Ca1a cells were stably transduced with FN or GFP as a control. These cells along with Ca1h cells as a reference were assessed by immunoblot for the indicated markers of EMT. Expression of β -tubulin served as a loading control. (H) Control (GFP) and FN expressing Ca1a cells were plated onto uncoated tessellated scaffolds and fibril formation was assessed. (I) Growth of control (GFP) and FN-expressing (FN) Ca1a cells was quantified 12-days post plating. Data are the mean (\pm SE) luminescence units normalized to the plated values (T0) for three independent experiments completed in triplicate, resulting in the indicated P value. (J) Control (GFP) and FN expressing Ca1a cells expressing firefly luciferase (1×10^6) were injected into the lateral tail vein of NRG mice and pulmonary tumor growth was tracked by bioluminescence. The mean (\pm SE) pulmonary bioluminescence values normalized to the injected values (n=4 per group) were quantified at the indicated time points, resulting in the indicated P value. (Inset) Representative lungs from mice receiving tail injections of control (GFP) or FN expressing Ca1a cells.

Figure 1

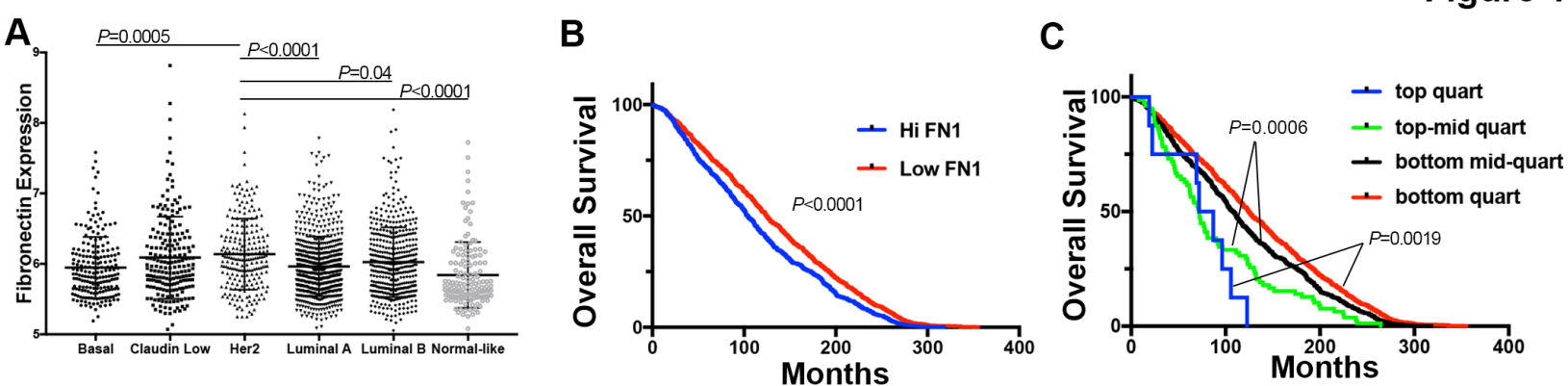


Figure 2

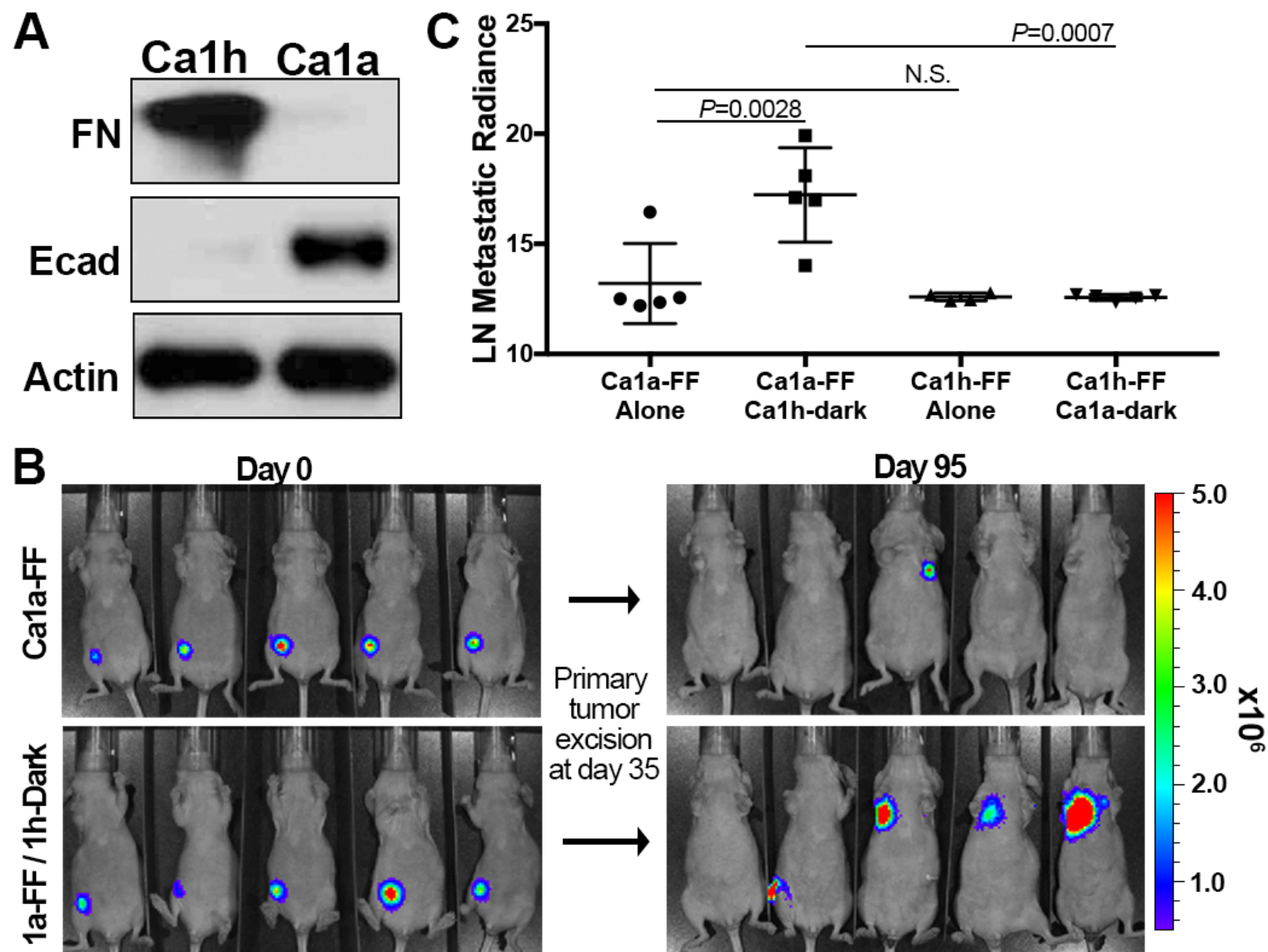
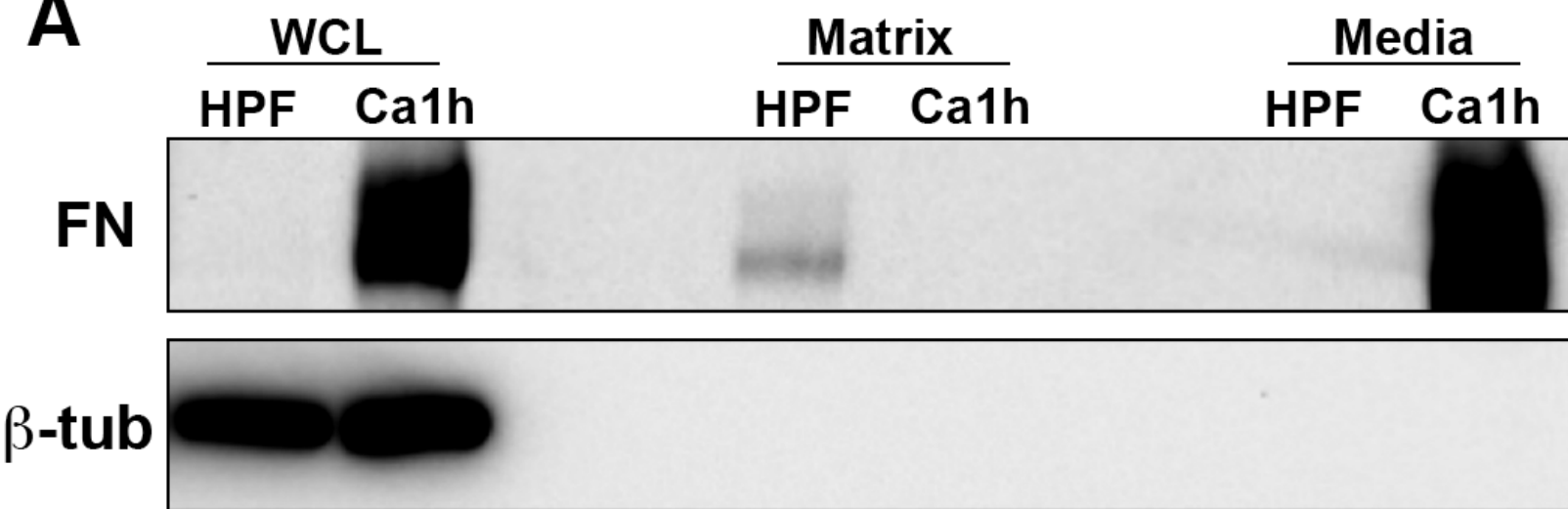


Figure 3

A



B

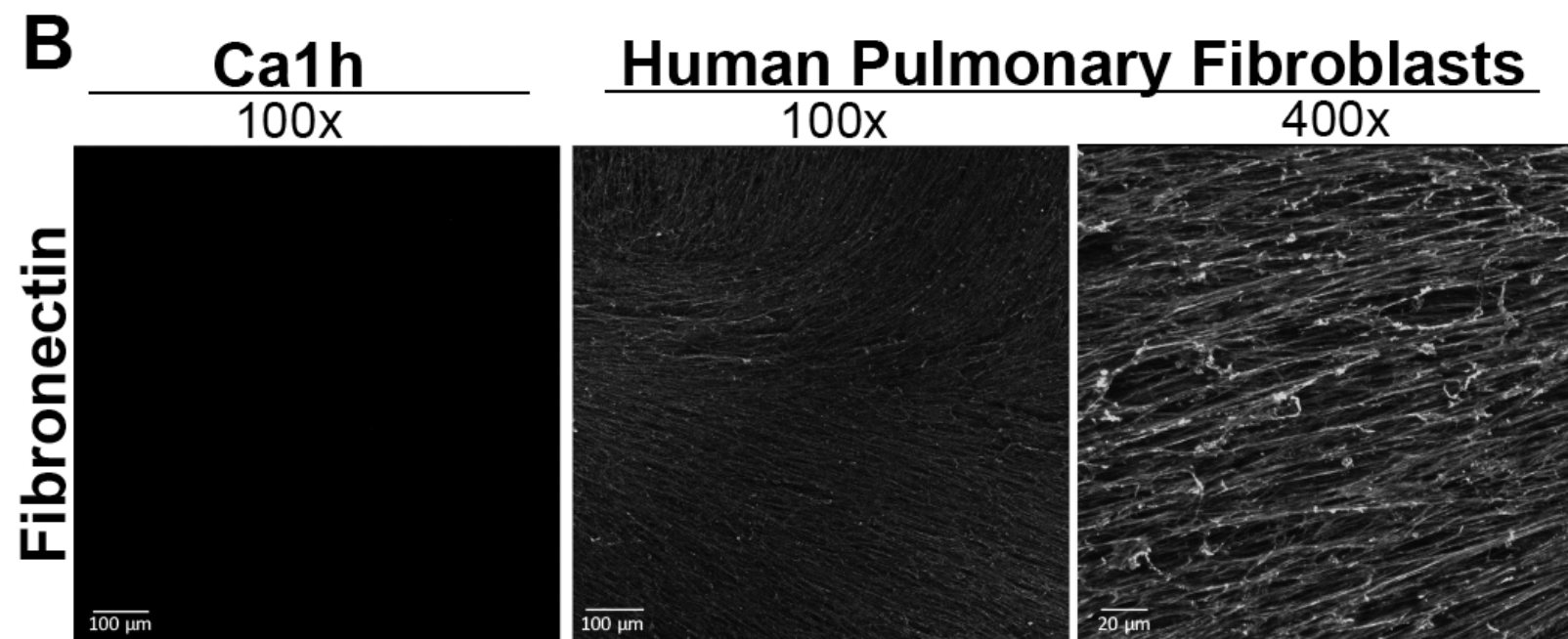


Figure 4

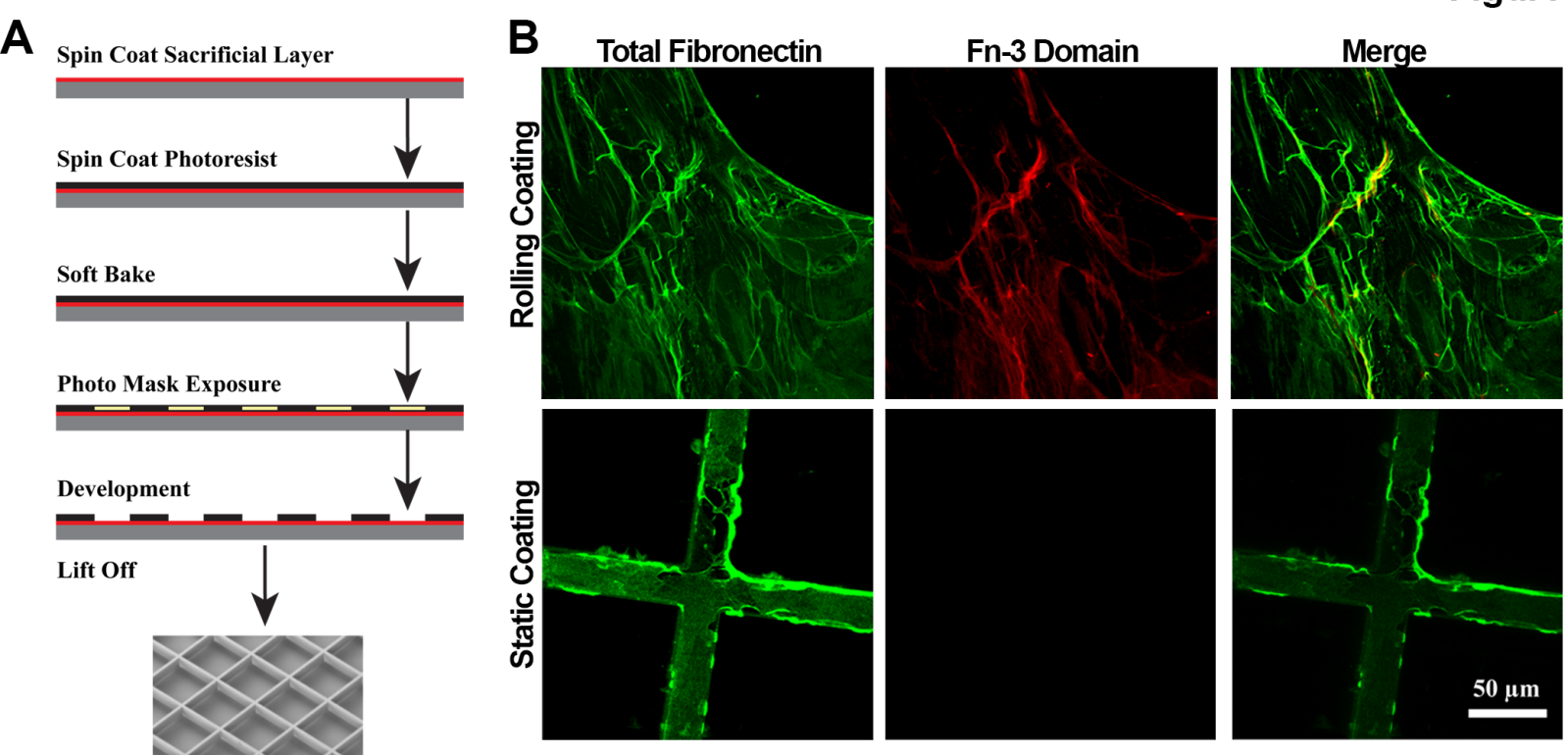


Figure 5

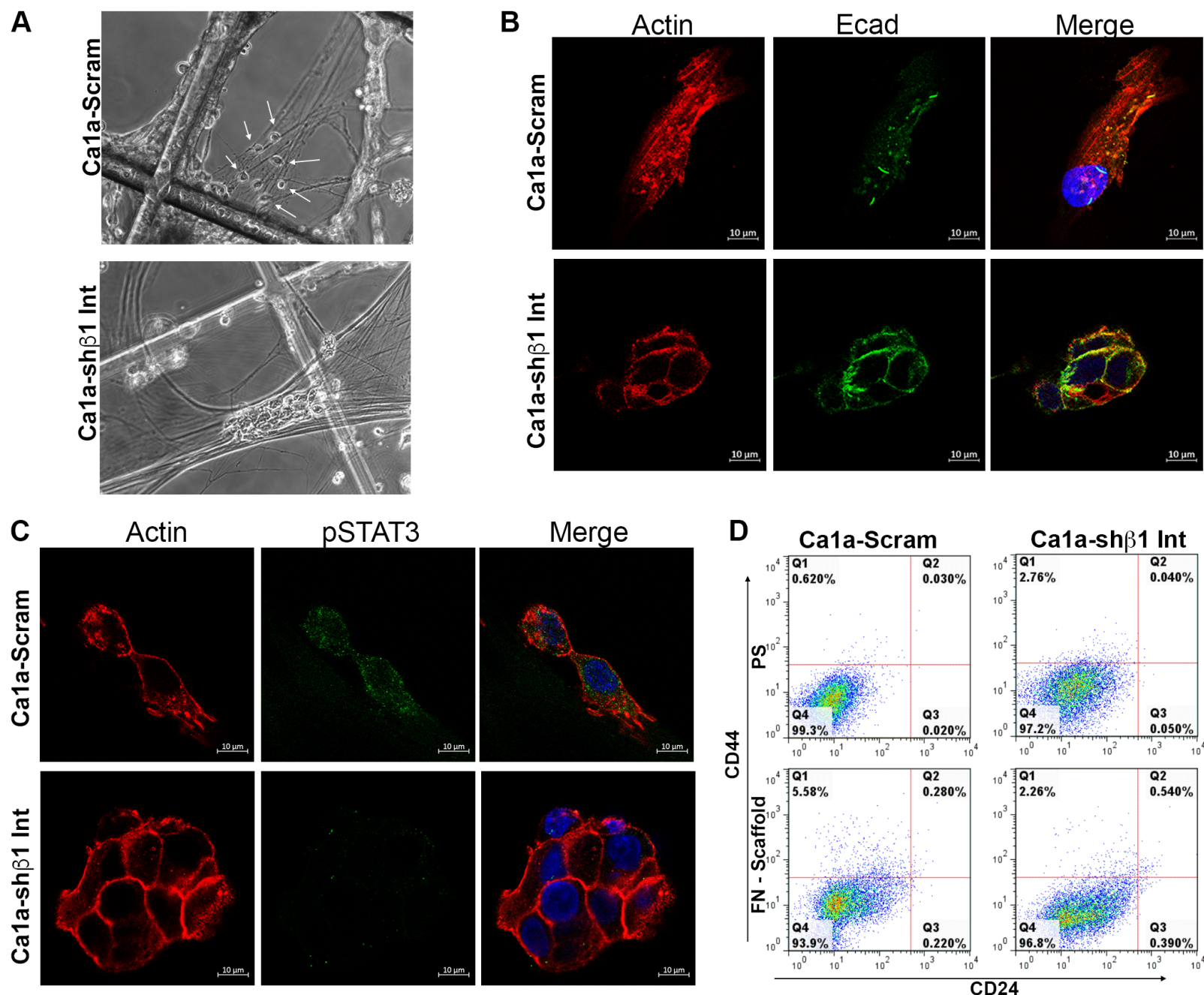


Figure 6

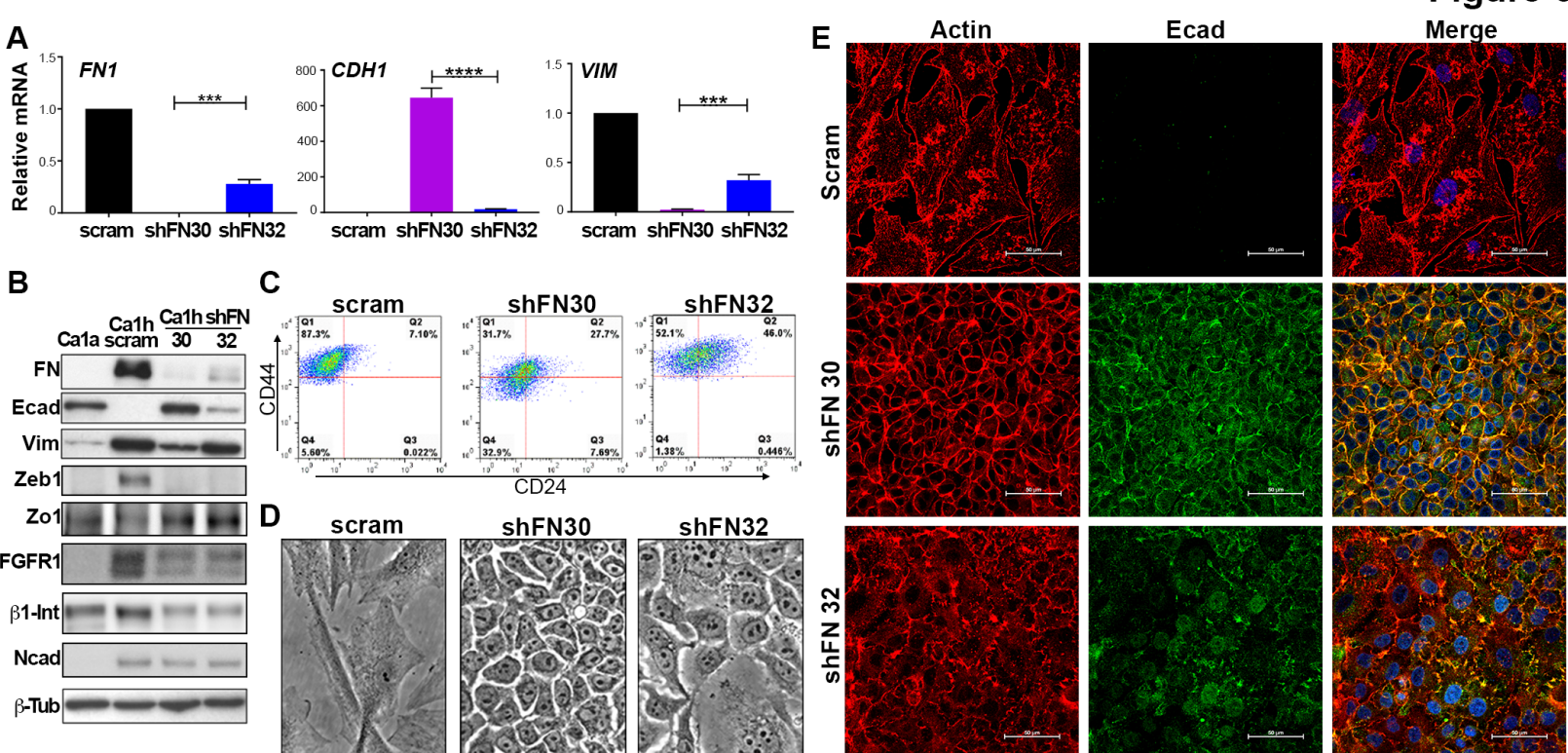


Figure 7

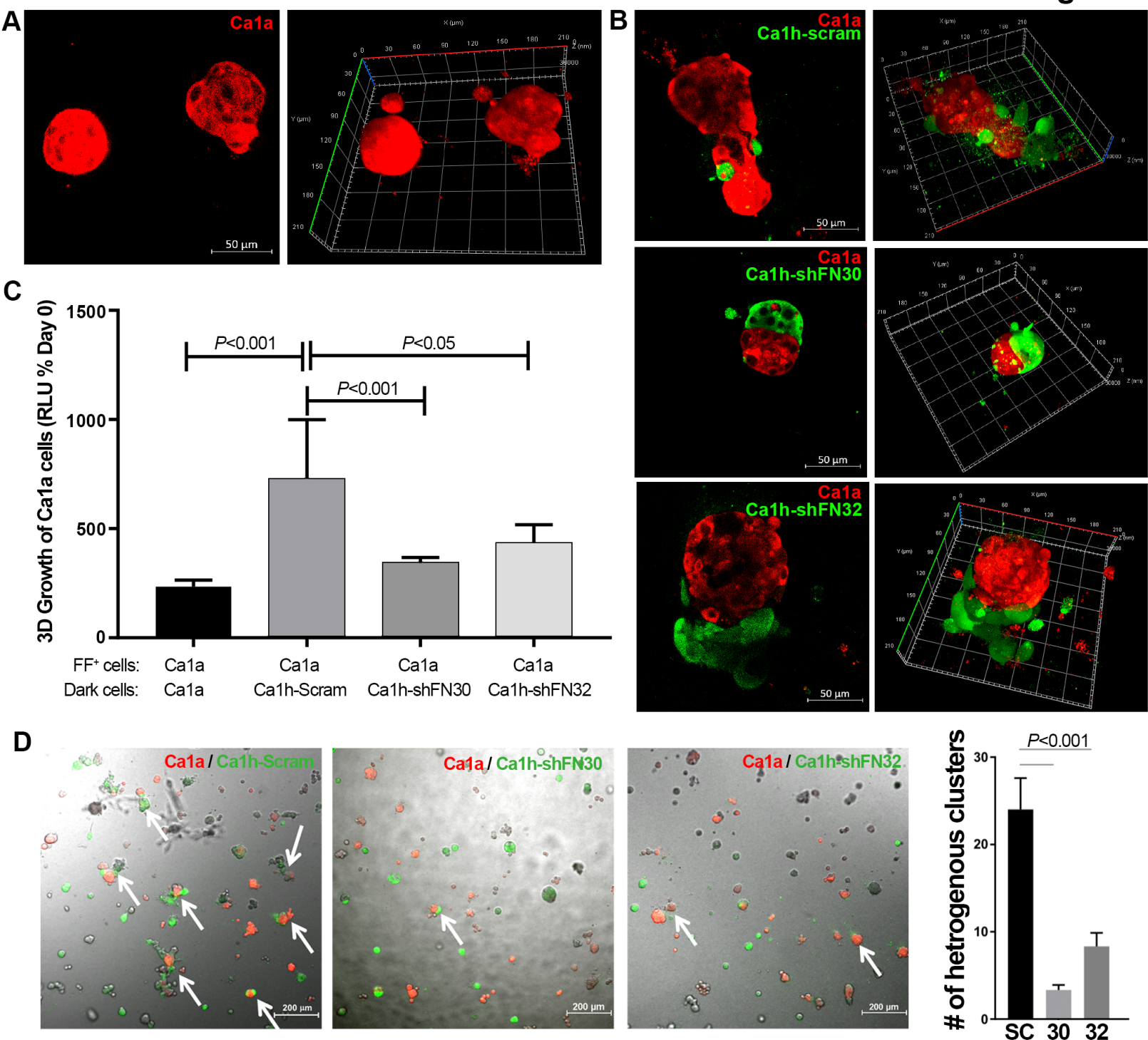
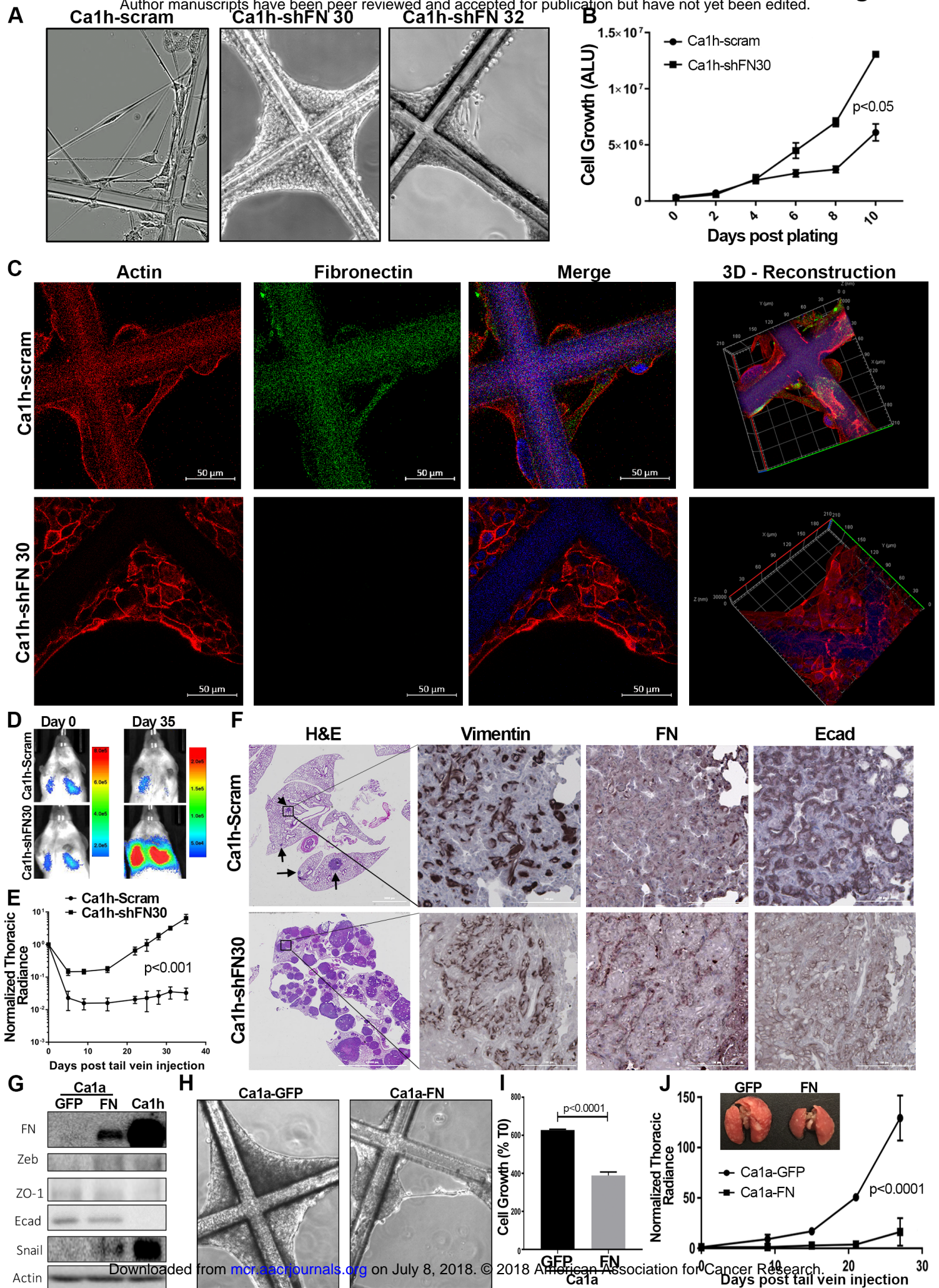


Figure 8

Author Manuscript Published OnlineFirst on June 22, 2018; DOI: 10.1158/1541-7786.MCR-18-0151
 Author manuscripts have been peer reviewed and accepted for publication but have not yet been edited.



Molecular Cancer Research

Autocrine Fibronectin Inhibits Breast Cancer Metastasis

Aparna Shinde, Sarah Libring, Aktan Alpsoy, et al.

Mol Cancer Res Published OnlineFirst June 22, 2018.

Updated version	Access the most recent version of this article at: doi:10.1158/1541-7786.MCR-18-0151
Supplementary Material	Access the most recent supplemental material at: http://mcr.aacrjournals.org/content/suppl/2018/06/22/1541-7786.MCR-18-0151.DC1
Author Manuscript	Author manuscripts have been peer reviewed and accepted for publication but have not yet been edited.

E-mail alerts	Sign up to receive free email-alerts related to this article or journal.
Reprints and Subscriptions	To order reprints of this article or to subscribe to the journal, contact the AACR Publications Department at pubs@aacr.org .
Permissions	To request permission to re-use all or part of this article, use this link http://mcr.aacrjournals.org/content/early/2018/06/22/1541-7786.MCR-18-0151 . Click on "Request Permissions" which will take you to the Copyright Clearance Center's (CCC) Rightslink site.